J. Plasma Phys. (2023), *vol*. 89, 905890114
Published by Cambridge University Press
doi:10.1017/S0022377823000144

Impact of wiggler magnetic field on wakefield generation and electron acceleration by Gaussian, super-Gaussian and Bessel–Gaussian laser pulses propagating in collisionless plasma

M. Abedi-Varaki [1],† **and M.E. Daraei**[2]

[1]Center for Physical Sciences and Technology, Savanorių 231, 02300 Vilnius, Lithuania

[2]Department of Atomic and Molecular Physics, Faculty of Basic Sciences, University of Mazandaran, Babolsar, Iran

(Received 5 November 2022; revised 30 January 2023; accepted 31 January 2023)

In this research, the process of electron acceleration and wakefield generation by Gaussian-like (GL), super-Gaussian (SG) and Bessel–Gaussian (BG) laser pulses through cold collisionless plasma in the presence of a planar magnetostatic wiggler are studied. Three different types of laser spatial profiles, GL, SG and BG, are considered. Additionally, using the hydrodynamics fluid equations, Maxwell's equations as well as the perturbation technique for GL, SG and BG laser pulses in the weakly nonlinear regime and in the presence of a planar magnetostatic wiggler, governing equations for analysing the laser wakefield and electron acceleration have been derived and compared correspondingly. In addition, the effect of some important factors, including the wiggler field strengths, laser intensity, pulse length, plasma electron density and laser frequency on the wakefield and the electron energy gain, have been investigated. Numerical results show that enhancing the wiggler magnetic field results in an increase in the amplitude of the wakefield. Furthermore, it is observed that in comparison with the wakefield amplitude excited by SG and GL laser pulses, the amplitude of the wakefield excited by BG laser pulse is larger when the wiggler field is enhanced. Moreover, it is realized that the type of the laser profile, selected laser parameters and wiggler magnetic field are the most decisive and effective factors in the wakefield amplitude and shape of wakefield generation through cold collisionless plasma. Also, it is seen that as the pulse length declines, the amplitude of the wakefield increases, and correspondingly the resonance positions shift to higher $(\Omega_w/\Omega_p)_{max}$ values.

Keywords: wakefield generation, electron acceleration, wiggler magnetic field, laser pulse

1. Introduction

Recently, many researchers have been attracted to and have shown great interest in investigating the interaction of laser pulses with plasma due to the significant advances in the production of short and high-intensity laser pulses (Hooker *et al.* 2007; Joshi 2007; Lundh *et al.* 2011; Hooker 2013; Abedi-Varaki & Jafari 2017*a*; Abedi-Varaki 2018*a*).

† Email address for correspondence: M.abedi.varaki@gmail.com

One of the areas of interest for researchers is the study into the effects of external fields such as the wiggler field and the uniform magnetic fields on the interactions of intense laser pulses with plasma. These fields have a centralizing role on the electron beam that is employed to accelerate within the plasma (Abedi-Varaki 2017; Abedi-Varaki & Jafari 2017*a*,*b*, 2018*a*,*b*,*c*; Abedi-Varaki & Panahi 2019; Gopal *et al.* 2021*a*). The electron acceleration in the laser–plasma interaction leads to nonlinear effects such as self-focusing, self-modulation, filamentation, second-harmonic generation, terahertz radiation generation and so on. In fact, nonlinear effects cause changes in the distribution of the input pulse intensity of the laser, which is applied in advanced technologies such as laser fusion, laser-plasma accelerators, laser ablation, X-ray lasers and inertial confinement fusion (ICF) (Abedi-Varaki & Jafari 2017*b*; Abedi-Varaki 2018*c*; 2020; Haines *et al.* 2020; Kautz, Phillips & Harilal 2020; Sherlock & Bissell 2020; Tajima & Malka 2020; Yadav, Gupta & Sharma 2020). To investigate electron acceleration in vacuum and plasmas in terms of theoretical and experimental aspects, several models have been proposed and developed (Abedi-Varaki 2018*b*; 2019; Gupta, Kant & Singh 2018; Caizergues *et al.* 2020; Yadav *et al.* 2020; Gopal, Gupta & Suk 2021*b*). The main focus has been on the production of high-energy particles, using ultra-short and ultra-intense lasers in the plasmas via compact ultrahigh gradient accelerators (Malik, Kumar, & Nishida 2007; Leemans *et al.* 2014; Litos *et al.* 2014). Generation of large amplitude plasma waves has been studied under several schemes and in numerous accelerators such as the plasma wakefield accelerator, laser wakefield accelerator (LWFA), resonant laser-plasma accelerator and the self-modulated laser wakefield accelerator (SMLWFA) (Lindberg *et al*. 2004; Hooker *et al.* 2007; Chen *et al.* 2009; Esarey, Schroeder & Leemans 2009; Jha, Saroch & Mishra 2013; Gupta *et al.* 2014; Albert *et al.* 2017). Recently, laser-plasma accelerators have been investigated from both an experimental and theoretical perspective. Tajima and Dawson (1979) studied laser-plasma accelerators. They found that the structures of wakes and sheaths in plasma are in conflict. When the large amplitude of wakefields involves collective resonance oscillations of the eigenmode of the entire plasma electrons, the wake phase velocity $\sim c$ and ultrafastness of the laser pulse introduce the wake stability and rigidity. When the phase velocity declines, wakefields turn into sheaths more suitable for ion acceleration. The outcomes of a nonlinear plasma wakefield accelerator (PWFA), high transformer ratio experiment has been reported by Roussel *et al.* (2020) applying high-charge, longitudinally asymmetric drive beams in a plasma cell. Moreover, single-shot wakefield measurements of a PWFA in the nonlinear regime by controlling over-drive beam shaping have also been illustrated in their experiment. A recorded transformer ratio of 7.8 ± 2.3 from a linearly ramped beam and the observation of a near uniform decelerating field for a drive beam with a parabolic head are two main outcomes of their experimental investigations. Some initial applications that probably came into view from plasma-based accelerator research have been examined by Joshi, Corde & Mori (2020). These applications include incoherent directional X-ray beams for science and technology, electron beam radiotherapy, near single cycle continuously tunable infrared pulses for spectroscopy as well as non-perturbative quantum electrodynamics enabled by plasma-based accelerator electron beams. The progression of these near-term applications has been promised and anticipated in the next decades, performing coordinated attempts. Emittance preservation through density ramp matching sections in a plasma wakefield accelerator has been studied by Zhao *et al.* (2020). It has been realized that the beam emittance can be preserved under the matching condition even while the beam has an initial energy spread.

In this article, we intend to investigate the influence of a wiggler magnetic field on electron acceleration and the wakefield produced resulting from GL, SG and BG laser

https://doi.org/10.1017/S0022377823000144 Published online by Cambridge University Press

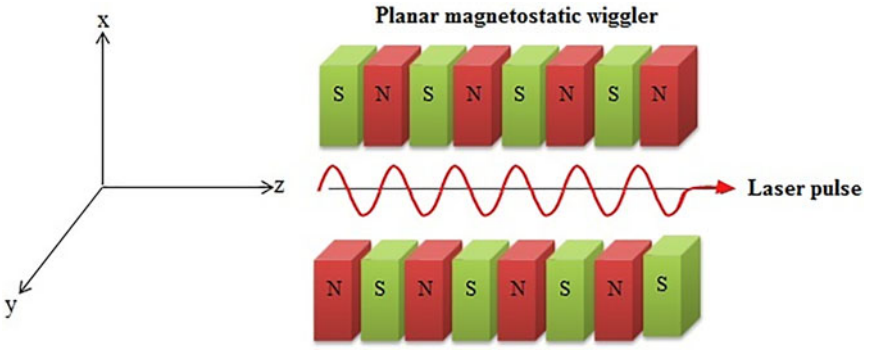

FIGURE 1. Schematic illustration of laser pulse trajectory in the presence of a planar magnetostatic wiggler.

pulses in plasma. The main body of the paper is divided into three sections. Section 2 refers to the derivation of fundamental equations and methods for the analysis of the laser wakefield in GL, SG and BG of laser pulses. The numerical results for wakefield properties on the electron acceleration are achieved and analysed in § 3. Finally, § 4 is devoted to the conclusions of the research.

2. Fundamental equations for analysis of laser wakefield

Propagation of electromagnetic waves through plasma has been considered in the presence of a planar magnetostatic wiggler in a weakly nonlinear regime. Our considered physical configuration comprises an intense laser pulse propagating through a cold collisionless plasma containing a periodic planar wiggler field ($\boldsymbol{B}_w = B_w \hat{e}_y$). The wiggler field can be expressed as (Abedi-Varaki & Jafari 2017*c*, 2017*d*, 2018*a*)

$$\boldsymbol{B}_w = B_w \sin(k_w z)\hat{e}_y, \tag{2.1}$$

where B_w and $k_w = 2\pi/\lambda_w$ are the amplitude and wavenumber of the wiggler field, respectively. A schematic illustration of this configuration is shown in figure 1.

Applying the following equations in plasma, a laser–plasma interaction in a nonlinear regime and in the presence of a wiggler field is yielded as follows:

$$\frac{\partial \boldsymbol{p}}{\partial t} + (\boldsymbol{v}\cdot\nabla)\boldsymbol{p} = -e[\boldsymbol{E} + \boldsymbol{u}\times(\boldsymbol{B}+\boldsymbol{B}_w)], \tag{2.2}$$

$$\nabla\times\boldsymbol{B} = \mu_0\left(\boldsymbol{J} + \varepsilon_0\frac{\partial \boldsymbol{E}}{\partial t}\right), \tag{2.3}$$

$$\nabla\times\boldsymbol{E} = -\frac{\partial \boldsymbol{B}}{\partial t}, \tag{2.4}$$

$$\boldsymbol{J} = -n_e e\boldsymbol{u}, \tag{2.5}$$

$$\frac{\partial n_e}{\partial t} + \nabla\cdot(n_e\boldsymbol{u}) = 0, \tag{2.6}$$

$$\nabla\cdot\boldsymbol{E} = \frac{e(n_i - n_e)}{\varepsilon_0}, \tag{2.7}$$

in which $\boldsymbol{E} = E(\zeta)\hat{e}_x$ and $\boldsymbol{B} = B(\zeta)\hat{e}_y$ are the electric and magnetic fields of an electromagnetic wave, n_e stands for the density of an electron, $\boldsymbol{J}$ is the current density of

https://doi.org/10.1017/S0022377823000144 Published online by Cambridge University Press

electrons of plasma, e refers to the magnitude of electron charge,$\boldsymbol{u}$ is the electron velocity and $\boldsymbol{p} = \gamma m\boldsymbol{u}$ denotes the relativistic momentum where the relativistic Lorentz factor (γ) can be shown as (Abedi-Varaki & Kant 2022)

$$\gamma = \left(1 - \left(\frac{u}{c}\right)^2\right)^{-1/2} = \sqrt{1 + \left(\frac{p}{mc}\right)^2}. \tag{2.8}$$

Considering the fact that the mass of the electron is lighter than the ion mass, the motion of the ion can be supposed to be negligible and the corresponding plasma can be considered in an equilibrium state. In this condition, plasma density n_0 and drift velocity $\boldsymbol{u}_0$ are constant and zero, respectively. Additionally, the laser pulse propagation is considered in the z-axis direction and the plasma electron density is mentioned as $n_e = n_0 + n'_e$, where n'_e is the electron density perturbation due to the laser pulse. As all the characteristics depend only on $\zeta = z - u_g t$ and by using the weakly nonlinear regime where$u_z \gg u_x$, the result is

$$p_z = mu_z\left(1 - \left(\frac{u_x + u_z}{c}\right)^2\right)^{-1/2} \approx mu_z\left(1 - \left(\frac{u_z}{c}\right)^2\right)^{-1/2} \approx mu_z \tag{2.9}$$

and

$$p_x = mu_x\left(1 - \left(\frac{u_x + u_z}{c}\right)^2\right)^{-1/2} \approx mu_x\left(1 - \left(\frac{u_x}{c}\right)^2\right)^{-1/2} \approx mu_x. \tag{2.10}$$

Applying the perturbation technique along with (2.1)–(2.7), while the wiggler field is present, will result in

$$-u_g\frac{\partial n'_e}{\partial \zeta} + n_0\frac{\partial u_x}{\partial \zeta} + u_x\frac{\partial n'_e}{\partial \zeta} + n'_e\frac{\partial u_x}{\partial \zeta} = 0, \tag{2.11}$$

$$-u_g\frac{\partial u_z}{\partial \zeta} + u_x\frac{\partial u_z}{\partial \zeta} = -\frac{e}{m}E + \frac{e}{m}u_xB + \Omega_w u_x c\sin(k_w z), \tag{2.12}$$

$$-u_g\frac{\partial u_x}{\partial \zeta} + u_x\frac{\partial u_x}{\partial \zeta} = \frac{e}{m}\frac{\partial \varphi_{wf}}{\partial \zeta} - \frac{e}{m}u_zB - \Omega_w u_z c\sin(k_w z), \tag{2.13}$$

$$\frac{\partial E}{\partial \zeta} = u_g\frac{\partial B}{\partial \zeta}, \tag{2.14}$$

$$\frac{\partial B}{\partial \zeta} = +\mu_0(n_0 + n'_e)eu_z + \frac{u_g}{c^2}\frac{\partial E}{\partial \zeta}, \tag{2.15}$$

$$\frac{\partial^2 \varphi_{wf}}{\partial^2 \zeta} = \frac{en'_e}{\varepsilon_0}, \tag{2.16}$$

in which $u_g = c(1 - \Omega_p^2/\Omega^2)^{1/2}$, $\Omega_w = eB_w/mc$ and $\Omega_p = (n_0e^2/m\varepsilon_0)^{1/2}$ are the group velocity, the wiggler frequency and the plasma frequency, respectively. The following equation can be derived by using (2.11)–(2.16):

$$-\frac{m}{e}\frac{u_g^2}{(n_0 + n'_e)}\frac{\partial n'_e}{\partial \zeta} = \frac{\partial \varphi_{wf}}{\partial \zeta} - \frac{u_zE(\zeta)}{u_g} - \Omega_w u_z c\sin(k_w z). \tag{2.17}$$

https://doi.org/10.1017/S0022377823000144 Published online by Cambridge University Press

Using the weakly nonlinear regime and considering small perturbations ($n_e' \ll n_0$), derivations will be as follows:

$$\frac{n'_e}{n_0} = -\frac{e}{mu_g^2}\varphi_{wf} + \frac{e}{mu_g^3}\int u_z E(\zeta)\partial\zeta + \frac{\Omega_w c \sin(k_w z)}{u_g^2}\int u_z \partial\zeta . \tag{2.18}$$

Integration of (2.18) by using (2.14)–(2.16) under the condition that n_e', u_x and u_z vanish as $|\zeta| \to \infty$ leads to wake potential as

$$\frac{\partial^2\varphi_{wf}}{\partial^2\zeta} + k_p^2\varphi_{wf} - \left[\left(\frac{e(\beta^2-1)}{2mu_g^2}\right)\left(E^2(\zeta) + \frac{2\Omega_w cm\sin(k_w z)E(\zeta)u_g}{e}\right)\right] = 0, \tag{2.19}$$

where $\beta = c/u_g$ and $k_p = \Omega_p/u_g = 2\pi/\lambda_p$ is the plasma wavenumber. Equation (2.19) generally represents the wake potential. As a matter of fact, the wake potential equation has a dependence on the external magnetic field, the electric field and the group velocity of the laser pulse. Furthermore, the force term that relates to the pondermotive force and drives the wakefield is indicated via the last term of (2.19). For formulating the electron acceleration and the interaction between electrons and the wakefield, (2.2) is considered as

$$\frac{\mathrm{d}p}{\partial t} = -eE_{wf}(\zeta). \tag{2.20}$$

For simplifying the mathematical processes, the variable $\eta = k_p(\zeta - L/2)$ which is associated with the wakefield phase has been introduced. Considering the one-dimensional motion of electron and taking $\zeta = z - u_g t$, we can achieve following relations:

$$\frac{\mathrm{d}\gamma}{\mathrm{d}t} = -\frac{epE_{wf}(\eta)}{\gamma m^2 c^2}, \quad \frac{\mathrm{d}\eta}{\mathrm{d}t} = k_p\left[\frac{c}{\gamma}(\sqrt{\gamma^2-1}) - u_g\right]. \tag{2.21a,b}$$

As a consequence, dividing $\mathrm{d}\gamma/\mathrm{d}t$ by $\mathrm{d}\eta/\mathrm{d}t$ and taking into account $\mathrm{d}z/\mathrm{d}t = u_z = c(1-1/\gamma^2)^{1/2}$ and their integration will consequently result in

$$\gamma - \gamma_0 - \frac{1}{\beta}\left(\left(\sqrt{\gamma^2-1}\right) - \left(\sqrt{\gamma_0^2-1}\right)\right) = \frac{-e}{k_p mc^2}\int E_{wf}(\eta)\,\mathrm{d}\eta. \tag{2.22}$$

Equation (2.22) represents the general equation that governs the electron acceleration in the wakefield. By assuming the initial value γ as γ_0 at $\zeta = 0$ and by integrating the above equation, $\Delta\gamma$ can be expressed as

$$\Delta\gamma = \frac{-e}{k_p mc^2\left(1-\frac{1}{\beta}\right)}\int E_{wf}(\eta)\,\mathrm{d}\eta. \tag{2.23}$$

Thus, the electron energy gain is achieved by the electron acceleration in the wakefield excited by the laser pulses by employing $\Delta W = mc^2\Delta\gamma$.

The main goal of this paper is to focus on the electron acceleration in the wakefield excited by GL, SG and BG laser pulses in the presence of a planar magnetostatic wiggler.

https://doi.org/10.1017/S0022377823000144 Published online by Cambridge University Press

2.1. *GL laser pulse*

The profiles of the field distributions of the GL laser pulse are given as

$$E_{GL}(\zeta) = E_0 \exp\left[-\frac{\left(\zeta - \frac{L}{2}\right)^2}{r_0^2}\right] \quad 0 \le \zeta \le L, \tag{2.24}$$

in which E_0 is the maximum amplitude of the Gaussian electric field, L is the pulse length and r_0 is the laser pulse waist. By putting (2.24) in (2.19), the wakefield potential φ_{WGL} behind the GL can be extracted as

$$\varphi_{WGL} = \frac{\alpha_{GL}}{k_p} \sin k_p \left(\zeta - \frac{L}{2}\right). \tag{2.25}$$

Here, α_{GL} can be presented as

$$\alpha_{GL} = (0.88)\left[\frac{eE_0^2 r_0}{mu_g^2}(\beta^2 - 1)\right] \mathrm{e}^{-k_p^2 r_0^2/4} + (1.77)\left[\frac{E_0 \Omega_w r_0 c \sin(k_w z)}{u_g}(\beta^2 - 1)\right] \mathrm{e}^{-k_p^2 r_0^2/2}. \tag{2.26}$$

In addition, the wakefield of the GL laser pulse is given by

$$E_{WGL} = -\frac{\partial \varphi_{wf}}{\partial \zeta} = -\alpha_{GL} \cos k_p \left(\zeta - \frac{L}{2}\right). \tag{2.27}$$

The density perturbations behind the GL pulse can be achieved by using (2.19) in combination with the weakly nonlinear regime as

$$\left(\frac{n'_e}{n_0}\right)_{GL} = -\frac{e}{mk_p u_g^2}\left(\alpha_{GL} \sin k_p \left(\zeta - \frac{L}{2}\right) - \frac{ec^2 E_0^2}{2mk_p u_g^4} - \frac{\Omega_w E_0 c^3 \sin(k_w z)}{2k_p u_g^3}\right). \tag{2.28}$$

Additionally, the electron energy gain of GL laser pulse in the presence of a planar magnetostatic wiggler can be derived by replacing (2.27) in (2.23) as

$$\Delta W_{GL} = \frac{e\alpha_{GL} u_g}{\Omega_p\left(1 - \frac{1}{\beta}\right)}\left[\sin k_p \left(\zeta - \frac{L}{2}\right) + \sin\left(\frac{k_p L}{2}\right)\right]. \tag{2.29}$$

2.2. *SG laser pulse*

For this type of pulse, the profiles of the field distributions are taken as

$$E_{SG}(\zeta) = E_0 \exp\left[-\frac{\left(\zeta - \frac{L}{2}\right)^2}{r_0^2}\right] \quad 0 \le \zeta \le L. \tag{2.30}$$

Replacing (2.30) in (2.19) under the same conditions as § 2 will lead to the wakefield potential φ_{WSG} and E_{WSG} behind the SG as

$$\varphi_{WSG} = \frac{\alpha_{SG}}{k_p} \sin k_p \left(\zeta - \frac{L}{2}\right), \tag{2.31}$$

$$E_{WSG} = -\frac{\partial \varphi_{wf}}{\partial \zeta} = -\alpha_{SG} \cos k_p \left(\zeta - \frac{L}{2}\right). \tag{2.32}$$

https://doi.org/10.1017/S0022377823000144 Published online by Cambridge University Press

Furthermore, the generalized hyper-geometric function is introduced in the following equation (Górska & Penson 2013):

$$ {}_pF_q\left(\left.\begin{matrix}(a_p)\\(b_q)\end{matrix}\right| z\right) = \sum_{k=0}^{\infty} \frac{(a_1)_k (a_2)_k \cdots (a_p)_k}{(b_1)_k (b_2)_k \cdots (b_q)_k} \frac{z^k}{k!}. \tag{2.33} $$

Here, $b_j \neq 0, -1, -2, \ldots, j = 1, 2, \ldots q$. It is worth mentioning that $(a)_k = \Gamma(a + k)/\Gamma(a)$ stands for the Pochhammer symbol in which Γ is the gamma function. Employing (2.33) and mathematical processes, the coefficient of α_{SG} is obtained as (Hörmander 1967)

$$ \begin{aligned} \alpha_{SG} = {} & \frac{ec^2E_0^2}{2mu_g^4}\left[-r_0^3\left(\left(\frac{1.8}{r_0^2}\right){}_0F_2\left(\frac{1}{2}, \frac{3}{4}; \frac{k_p^4 r_0^4}{256}\right) + (0.3k_p^2){}_0F_2\left(\frac{5}{4}, \frac{3}{2}; \frac{k_p^4 r_0^4}{256}\right)\right)\right] \\ & + \frac{\Omega_w E_0 r_0 c^3 \sin(k_w z)}{u_g^3}\left[-r_0^3\left(\left(\frac{1.8}{r_0^2}\right){}_0F_2\left(\frac{1}{2}, \frac{3}{4}; \frac{k_p^4 r_0^4}{128}\right)\right.\right. \\ & \left.\left. + (0.3k_p^2){}_0F_2\left(\frac{5}{4}, \frac{3}{2}; \frac{k_p^4 r_0^4}{128}\right)\right)\right], \end{aligned} \tag{2.34} $$

where ${}_0F_2(a, b; c)$ is a hyper-geometric function. We can obtain the density perturbations behind the SG pulse by using (2.18) and employing (2.31) and (2.32) to get

$$ \left(\frac{n'_e}{n_0}\right)_{SG} = -\frac{e}{m\Omega_p u_g}\left(\alpha_{SG} \sin k_p\left(\zeta - \frac{L}{2}\right) - \frac{ec^2E_0^2}{2m\Omega_p u_g^3} - \frac{E_0\Omega_w c^3 \sin(k_w z)}{2\Omega_p u_g^2}\right). \tag{2.35} $$

As a result, we can compute the electron energy gain in the wakefield excited by SG laser pulse as

$$ \Delta W_{SG} = \frac{ec\alpha_{SG}}{\Omega_p(\beta - 1)}\left[\sin k_p\left(\zeta - \frac{L}{2}\right) + \sin\left(\frac{k_p L}{2}\right)\right]. \tag{2.36} $$

2.3. *BG laser pulse*

Finally, the case of wakefield excitation has been analysed with a BG laser pulse. The profiles of the field distributions of the BG laser pulse are given as follows (Li, Lee & Wolf 2004):

$$ E_{BG}(\zeta) = E_0 \exp\left[-\frac{\left(\zeta - \frac{L}{2}\right)^2}{r_0^2}\right] J_0\left(k\left(\zeta - \frac{L}{2}\right)\right) \quad 0 \leq \zeta \leq L, \tag{2.37} $$

in which k and J_0 are the transverse wavenumber and the zero-order Bessel function, respectively. Using (2.37), (2.19) will be obtained under the conditions that the wake potential is zero at the middle of pulse ($\zeta = L/2$) as

$$ \varphi_{WBG} = \frac{\alpha_{BG}}{k_p} \sin k_p\left(\zeta - \frac{L}{2}\right). \tag{2.38} $$

https://doi.org/10.1017/S0022377823000144 Published online by Cambridge University Press

Employing the expansion of Bessel function, the coefficient of α_{BG} in (2.38) is achieved as follows (Fallah & Khorashadizadeh 2019):

$$\alpha_{BG} = \frac{\sqrt{er_0}cE_0}{(5.65)mu_g^4}\left(1-\frac{1}{\beta^2}\right)\left[\left({}_1F_1\left(0,\frac{1}{2};\frac{k_p^2r_0^2}{8}\right)+\left(\frac{k^2r_0^2}{8}\right){}_1F_1\left(-1,\frac{1}{2};\frac{k_p^2r_0^2}{8}\right)\right.\right.$$
$$\left.\left.+(0.011)(k^4r_0^4){}_1F_1\left(-2,\frac{1}{2};\frac{k_p^2r_0^2}{8}\right)\right)\right]$$
$$\times\exp\left(-\frac{k_p^2r_0^2}{8}\right)+\frac{\Omega_wE_0r_0c^3\sin(k_wz)}{(0.44)u_g^3}\left(1-\frac{1}{\beta^2}\right)$$
$$\times\left[\left({}_1F_1\left(0,\frac{1}{2};\frac{k_p^2r_0^2}{4}\right)-\left(\frac{k^2r_0^2}{8}\right){}_1F_1\left(-1,\frac{1}{2};\frac{k_p^2r_0^2}{4}\right)\right)\right]\exp\left(-\frac{k_p^2r_0^2}{4}\right). \quad (2.39)$$

Here, ${}_1F_1(a,b;c)$ is the confluent hyper-geometric function. Furthermore, the wakefield of the BG laser pulse is calculated as

$$E_{WBG} = -\frac{\partial\varphi_{wf}}{\partial\zeta} = -\alpha_{BG}\cos k_p\left(\zeta-\frac{L}{2}\right). \quad (2.40)$$

By inserting (2.40) in (2.23), the electron energy gain of the GL laser pulse in the presence of a wiggler field is obtained as follows:

$$\Delta W_{SG} = \frac{ecu_g\alpha_{BG}}{\Omega_p(c-u_g)}\left[\sin k_p\left(\zeta-\frac{L}{2}\right)+\sin\left(\frac{k_pL}{2}\right)\right]. \quad (2.41)$$

Equation (2.41) denotes the electron energy gain in the wakefield produced by a BG laser pulse in the presence of a planar magnetostatic wiggler in cold collisionless plasma.

3. Numerical results and discussion

Analytical solutions of equations including Maxwell's equations, hydrodynamics fluid equations as well as perturbation technique for laser wakefields induced by GL, SG and BG laser pulses in the weakly nonlinear regime reveal that the amplitude of the wakefield depends on some parameters such as frequency, energy, intensity, length of laser pulses as well as wiggler field and plasma electron density. Thus, the influence of such parameters on the electron acceleration and wakefield is considered and investigated for three shapes of GL, SG and BG laser pulses in the presence of a planar magnetostatic wiggler. To study the mentioned parameters effects, laser frequency, laser intensity and plasma electron density are assumed as 2.4×10^{15} Hz, 3×10^{22} W m^{-2} and $n_0 = 2.5\times10^{24}$ m^{-3}, respectively, on the basis of a wavelength of $\lambda = 800$ nm.

As an outcome of the numerical results of this research, we will finally be able to understand and analyse how a wiggler magnetic field can result in considerable variations in the amplitude of the wakefield and also boost the energy of accelerated electrons in a cold collisionless plasma.

3.1. *Evaluation of GL, SG and BG wakefields*

3.1.1. *Influence of laser intensity*

As can be seen from figure 2(*a–c*), by considering different values of the laser intensity as 0.75×10^{22} W m^{-2}, 1.5×10^{22} W m^{-2}, 2.25×10^{22} W m^{-2} and 3×10^{22} W m^{-2}, the

https://doi.org/10.1017/S0022377823000144 Published online by Cambridge University Press

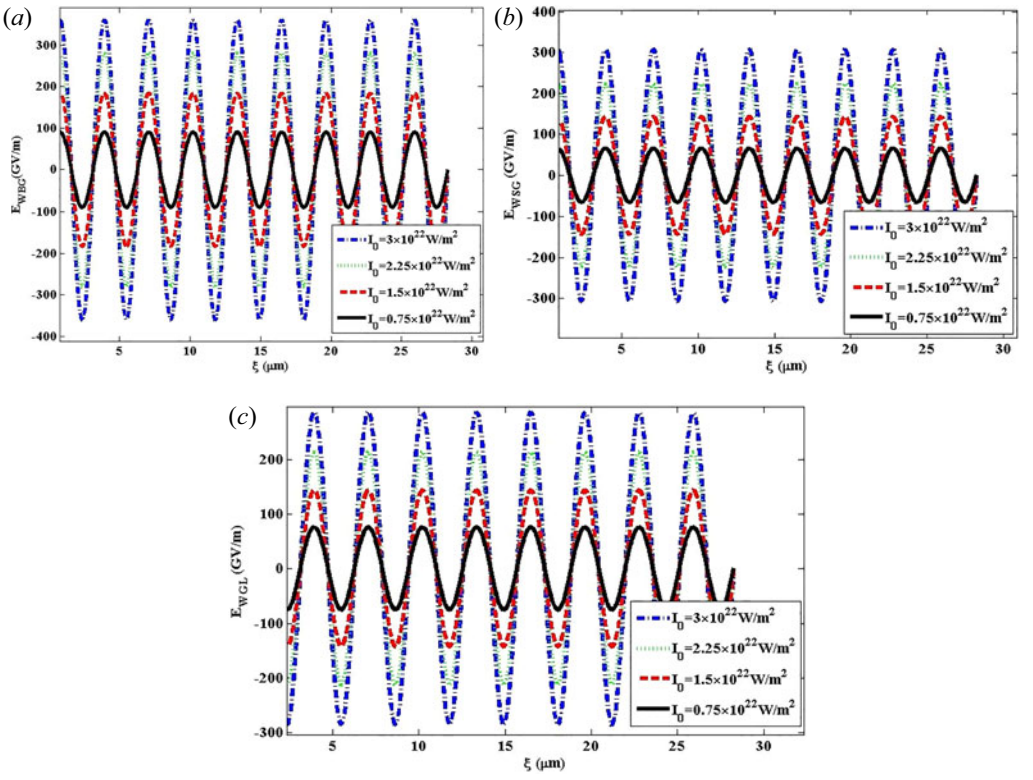

FIGURE 2. Variation of the wakefield versus the distance for (a) BG, (b) SG and (c) GL laser pulses at laser intensities of 0.75×10^{22} W m^{-2}, 1.5×10^{22} W m^{-2}, 2.25×10^{22} W m^{-2} and 3×10^{22} W m^{-2} when $B_w = 50$ T.

variation of the wakefield versus the distance for BG, SG and GL laser pulses in $B_w = 50$ T has been illustrated. It is clearly understood through these figures that an increase in laser intensity from 0.75×10^{22} W m^{-2} to 3×10^{22} W m^{-2} for three different shapes of BG, SG and GL laser pulses leads to an increase in the wakefield. Additionally, (2.28) and (2.35) disclose the direct association of the wakefield amplitude with E_0^2. As a result, it is promising that the higher intensity laser pulses will excite a larger amplitude owing to the larger density perturbations in collisionless plasma and correspondingly a larger wakefield will be generated.

3.1.2. *Influence of laser frequency*

Variation of the wakefield amplitude with respect to the laser frequency has been illustrated in figure 3(*a–c*) for BG, SG and GL laser pulses. It is worth mentioning that for this case, the intensity of the laser has been considered 3×10^{22} W m^{-2} and the wiggler field has different values of $B_w = 18$ T, 34 T, 50 T and 66 T. These curves clearly show that an increase in the wiggler magnetic field and laser frequency yields an increased wakefield amplitude. It sounds that the main reason for the growth in wakefield amplitude is the laser group velocity. In other words, the frequency of the laser pulse is completely dependent on the laser group velocity. It is deduced that a slight variation in group velocity of the laser pulse due to the laser frequency results in a more significant variation in factor $(\beta^2 - 1)$ that appears in (2.19). Additionally, it is inferred that with increasing laser group velocity for larger frequencies, the electron energy gain gets larger with enhancing laser frequency.

https://doi.org/10.1017/S0022377823000144 Published online by Cambridge University Press

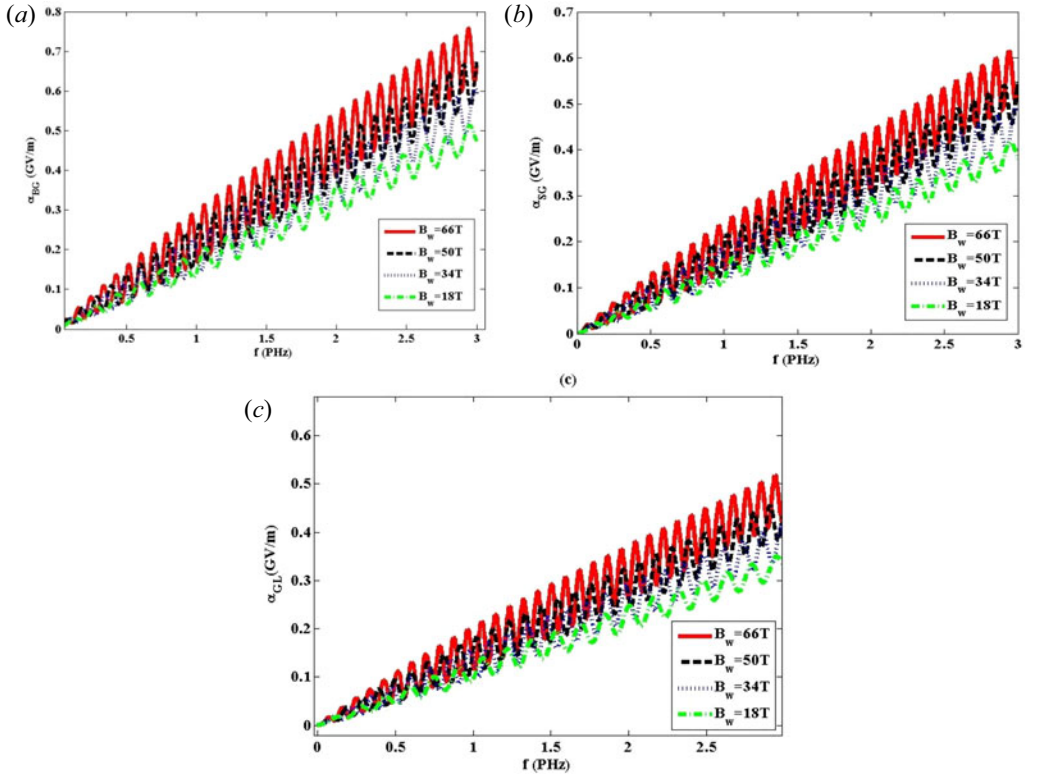

FIGURE 3. Variation of the wakefield amplitude versus the laser frequency for (a) BG, (b) SG and (c) GL laser pulses at laser intensity 3×10^{22} W m^{-2} for $B_w = 18$ T, 34 T, 50 T and 66 T.

It is important to emphasize that the electron energy gain is proportional to the factor $1/(\beta - 1)$. Moreover, a greater effectiveness of the wiggler field on the BG laser pulse in comparison with SG and GL laser pulses is the predominant outcome of this section.

3.1.3. *Influence of the electron energy gain*

Variation of the electron energy gain versus the plasma electron density and laser intensity for BG, SG and GL laser pulses in the presence of a wiggler magnetic field has been demonstrated in figures 4 and 5. It is obvious from figure 4(*a–c*) that the electron energy gain has first a sharp upward trend and then follows a moderate drop while the laser intensity is raised from 0.75×10^{22} W m^{-2} to 3×10^{22} W m^{-2} for BG, SG and GL laser pulses. Indeed, with increasing laser intensity, the difference in the electron energy gain has an increasing trend and eventually reaches a maximum of 18.88 MeV, 15.84 MeV and 13.64 MeV for a specific plasma electron density in BG, SG and GL laser pulses, respectively. In addition, it is specified that the electron energy gain has the largest amount for the BG laser pulse in comparison with SG and GL laser pulses. With consideration of figure 5, we will encounter an upward trend in electron energy gain for all three shapes of laser pulses while the laser intensity increases. To provide more details, the periodic behaviour is dominant and then the electron energy gain shows a considerable ascending trend to 511 MeV, 414 MeV and 322 MeV for BG, SG and GL laser pulses, respectively. Correspondingly, it can be comprehended that the electron accelerating force and subsequently the electron velocity increase as the wakefield amplitude increases,

https://doi.org/10.1017/S0022377823000144 Published online by Cambridge University Press

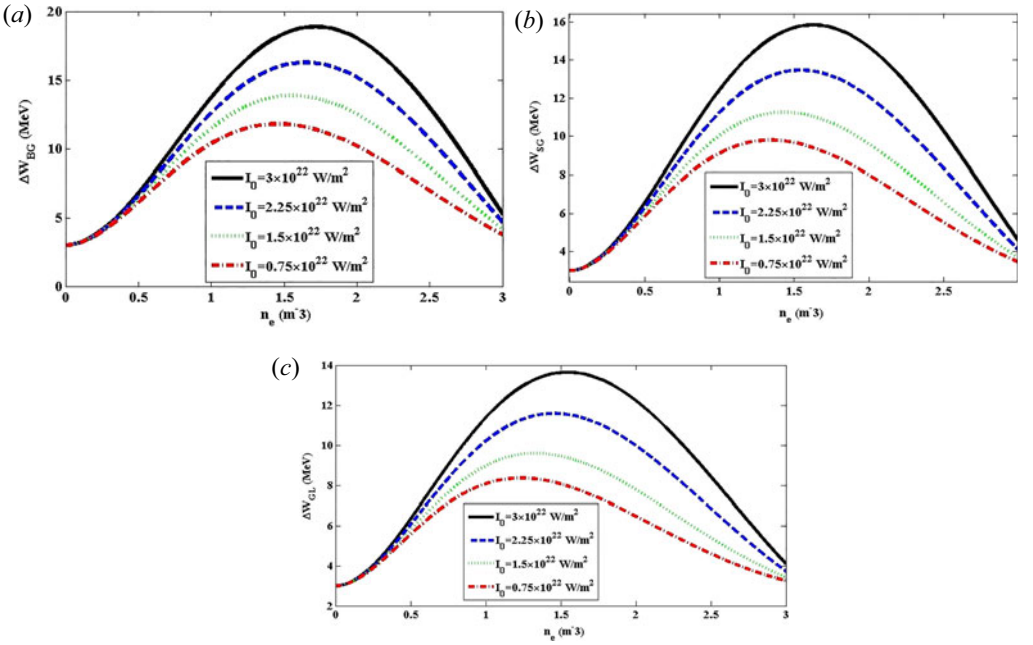

FIGURE 4. Variation of the electron energy gain versus the plasma electron density for (a) BG, (b) SG and (c) GL laser pulses. The chosen parameters are $\lambda = 0.8\ \mu$m, $B_w = 50$ T and $L = 25\ \mu$m.

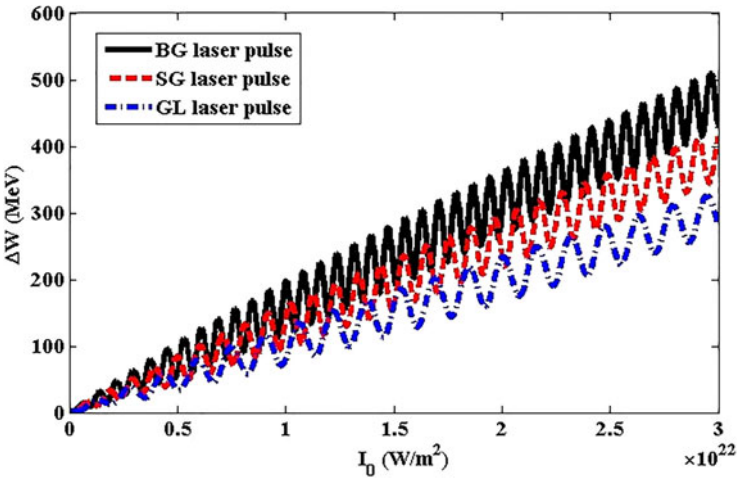

FIGURE 5. Variation of the electron energy gain versus the laser intensity for (a) BG (b) SG and (c) GL laser pulses. The chosen parameters are $\lambda = 0.8\ \mu$m, $B_w = 50$ T, $L = 25\ \mu$m and $n_0 = 2.5 \times 10^{24}$ m^{-3}.

which consequently results in a higher electron energy gain. Also, a comparison among the energy gain obtained in the wakefield excited by BG, SG and GL laser pulses in the presence of a planar magnetostatic wiggler reveals the trend $W_{BG} > W_{SG} > W_{GL}$ for the electron energy gain.

https://doi.org/10.1017/S0022377823000144 Published online by Cambridge University Press

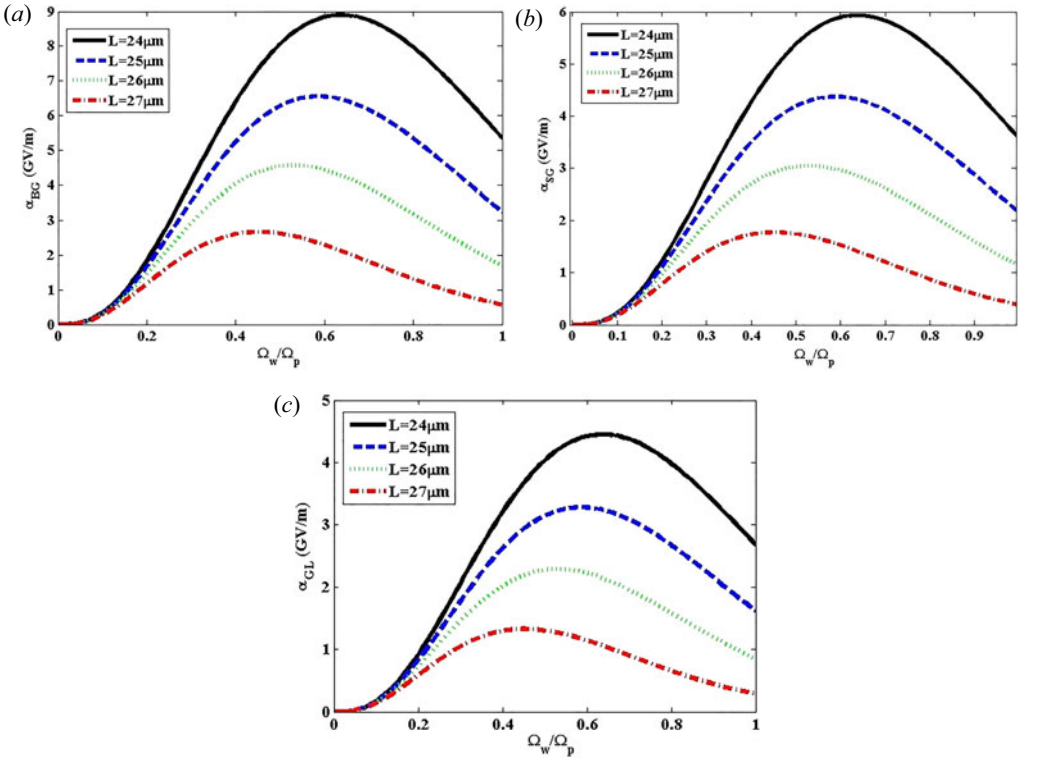

FIGURE 6. Variation of the wakefield amplitude versus the Ω_w/Ω_p at laser intensity 3×10^{22} W m^{-2} for (a) BG, (b) SG and (c) GL laser pulses for different values of $L = 24$ μm, 25 μm, 26 μm and 27 μm.

3.1.4. *Influence of pulse length*

Variation of the wakefield amplitude versus Ω_w/Ω_p for BG, SG and GL laser pulses at laser intensity 3×10^{22} W m^{-2} and different values of the pulse length as $L = 24$ μm, 25 μm, 26 μm and 27 μm is demonstrated in figures 6(*a*) and 6(*b*). It is understood from these figures that increasing the pulse length yields a decline in the wakefield amplitude so that $L = 27$ μm reaches minimum values of $\alpha_{BG} = 2.66$ GV m^{-1}, $\alpha_{SG} = 1.77$ GV m^{-1} and $\alpha_{GL} = 1.32$ GV m^{-1} at the resonance positions shift of $(\Omega_w/\Omega_p)_{min} = 0.46$, $(\Omega_w/\Omega_p)_{min} = 0.44$ and $(\Omega_w/\Omega_p)_{min} = 0.42$ for BG, SG and GL laser pulses, respectively. Additionally, the remarkable role of the pulse length in wakefield excitation has been revealed and has been shown that the amplitude of the wakefield is enhanced while the pulse length decreases, resulting in a shift to the higher number of resonant positions $(\Omega_w/\Omega_p)_{max}$.

3.1.5. *Influence of wiggler magnetic field*

Variation of the wakefield with respect to the distance at laser intensity $I_0 = 3 \times 10^{22}$ W m^{-2} for BG, SG and GL laser pulses has been demonstrated in figure 7(*a–c*). For this case, the wiggler magnetic field has different values of $B_w = 0$ T, 18 T, 34 T and 50 T. As shown, changes in the wiggler magnetic field have substantial effects on the amplitude of the wakefield. As analysed, although the overall behaviour of the wakefield does not change, the wakefield amplitude shows an increasing trend when the wiggler magnetic field increases. As can be seen, compared to the cases of SG and GL laser pulses, when

https://doi.org/10.1017/S0022377823000144 Published online by Cambridge University Press

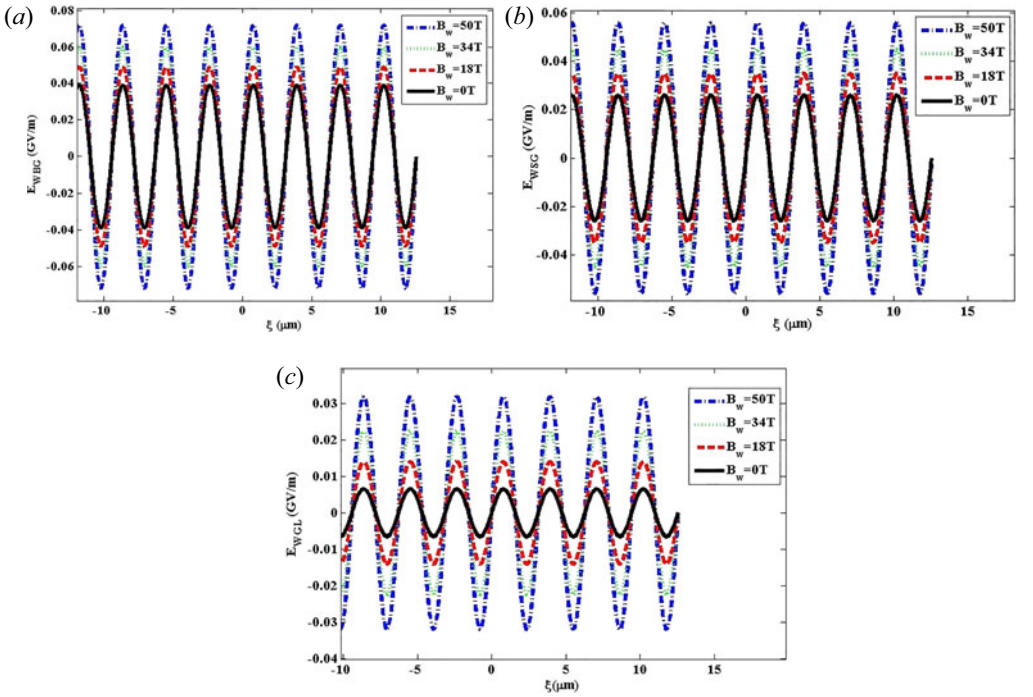

FIGURE 7. Variation of the wakefield versus the distance for (a) BG, (b) SG and (c) GL laser pulses at laser intensity 3×10^{22} W m^{-2} for different values of $B_w = 0$ T, 18 T, 34 T and 50 T.

the wiggler field is increased, the wakefield amplitude excited by the BG laser pulse will be larger. Moreover, (2.19) implies that the wake potential is related to the wiggler field. Hence, a rise in the wiggler field gives rise to a larger wakefield.

3.1.6. *Influence of the plasma electron density*

Variations of the wakefield versus the distance for BG, SG and GL laser pulses in $B_w = 50$ T and laser intensity $I_0 = 3 \times 10^{22}$ W m^{-2} have been illustrated in figure 8(*a–c*). In this case, the plasma electron density has different values of 0.62×10^{24} m^{-3}, 1.25×10^{24} m^{-3}, 1.87×10^{24} m^{-3} and 2.5×10^{24} m^{-3}. As evident for the BG laser pulse, the wakefield increases to 527 GV/m as the plasma electron density increases. Moreover, it is comprehensible that compared to SG and GL laser pulses, the wakefield excited by the BG laser pulse is stronger. In fact, as can be realized, lower densities represent a larger electron bunch, and alteration in the background electron density leads to variations in the amplitude of the wakefield. Moreover, it is found that the plasma electron density can be affected by the wakefield position behind the laser pulse.

4. Concluding remarks

In this work, considering BG, SG and GL laser pulses propagating in a cold collisionless plasma, the effect of a wiggler magnetic field on wakefield generation and electron acceleration has been. Additionally, using the hydrodynamics fluid equations, Maxwell's equations as well as the perturbation technique for GL, SG and BG laser pulses in the weakly nonlinear regime and in the presence of a planar magnetostatic wiggler, governing equations on the wakefield generation and electron acceleration have been achieved and compared correspondingly. Additionally, the wakefield and the electron energy gain are two important components where their affectability through the wiggler

https://doi.org/10.1017/S0022377823000144 Published online by Cambridge University Press

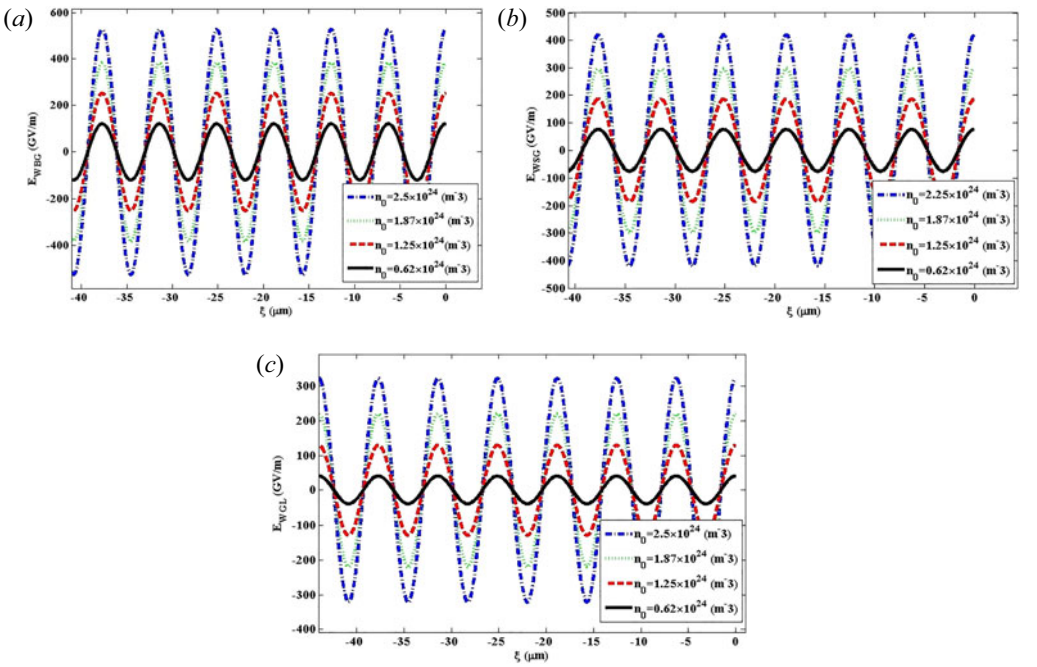

FIGURE 8. Variation of the wakefield versus the distance for (a) BG, (b) SG and (c) GL laser pulses. The chosen parameters are B_w=50 T, I_0=3 × 10^{22} W m^{-2} for different values of n_0=0.62 × 10^{24} m^{-3}, 1.25 × 10^{24} m^{-3}, 1.87 × 10^{24} m^{-3} and 2.5 × 10^{24} m^{-3}.

field strengths, laser intensity, pulse length, plasma electron density and laser frequency has been investigated. Numerical results show that increasing the wiggler magnetic field leads to an ascent in the amplitude of the wakefield. Moreover, it has been recognized that in comparison with the wakefield amplitude excited by SG and GL laser pulses, the amplitude of the wakefield excited by a BG laser pulse is larger when the wiggler magnetic field is increased. Furthermore, it is realized that the type of the laser profile, selected laser parameters and wiggler magnetic field are the most decisive and key factors in the wakefield amplitude and shape of the wakefield generation through cold collisionless plasma. Additionally, it has been observed that when the pulse length is enhanced, the impact of the wiggler field on the wakefield amplitude in the presence of the BG, SG, and GL laser pulses is considerable. In addition, it has been observed that as the pulse length declines, the amplitude of the wakefield increases, and correspondingly the resonance positions shift to higher $(\Omega_w/\Omega_p)_{max}$ values. Lastly, it is worth mentioning for our ultimate part of the conclusion that the peak of the wakefield can be shifted by adjusting the laser parameters and wiggler field strength, and, correspondingly, a significant change is observed in the wakefield generation and electron acceleration.

Acknowledgements

Editor Dmitri Uzdensky thanks the referees for their advice in evaluating this article.

Declaration of interests

The authors report no conflict of interest.

Data availability

The data that supports the findings of this study are available in the paper.

https://doi.org/10.1017/S0022377823000144 Published online by Cambridge University Press

REFERENCES

ABEDI-VARAKI, M. 2017 The effect of the wiggler magnetic field strength on the self-focusing of an intense laser pulse propagating through a magnetized non-Maxwellian plasma. *Phys. Plasmas* **24** (12), 122308.

ABEDI-VARAKI, M. 2018*a* Effects of the wiggler field on the terahertz radiation generated by intense laser beam in collisionless magnetoplasma. *UPB Sci. Bull.* A- *Appl. Math. Phys.* **80** (2), 289.

ABEDI-VARAKI, M. 2018*b* Electron acceleration by a circularly polarized electromagnetic wave publishing in plasma with a periodic magnetic field and an axial guide magnetic field. *Mod. Phys. Lett.* B **32** (20), 1850225.

ABEDI-VARAKI, M. 2018*c* Enhanced THz radiation generation by photo-mixing of tophat lasers in rippled density plasma with a planar magnetostatic wiggler and s-parameter. *Phys. Plasmas* **25** (2), 023109.

ABEDI-VARAKI, M. 2019 Electron acceleration of a surface wave propagating in wiggler-assisted plasma. *Mod. Phys. Lett.* B **33** (20), 1950267.

ABEDI-VARAKI, M. 2020 Effect of obliquely external magnetic field on the intense laser pulse propagating in plasma medium. *Intl J. Mod. Phys.* B **34** (07), 2050044.

ABEDI-VARAKI, M. & JAFARI, S. 2017*a* Nonlinear interaction of intense left-and right-hand polarized laser pulse with hot magnetized plasma. *J. Plasma Phys*. **83** (4), 655830401.

ABEDI-VARAKI, M. & JAFARI, S. 2017*b* Relativistic self-focusing of an intense laser pulse with hot magnetized plasma in the presence of a helical magnetostatic wiggler. *Phys. Plasmas* **24** (8), 082309.

ABEDI-VARAKI, M. & JAFARI, S. 2017*c* Self-focusing and de-focusing of intense left-and right-hand polarized laser pulse in hot magnetized plasma in the presence of an external non-uniform magnetized field. *Braz. J. Phys*. **47** (5), 473.

ABEDI-VARAKI, M. & JAFARI, S. 2017*d* Self-focusing and de-focusing of intense left and right-hand polarized laser pulse in hot magnetized plasma: laser out-put power and laser spot-size. *Opt.-Intl J. Light Electron. Opt*. **142**, 360.

ABEDI-VARAKI, M. & JAFARI, S. 2018*a* The effects of helical magnetostatic wiggler on the modulation instability of a laser pulse propagating through a hot magnetoplasma. *Opt.-Intl J. Light Electron. Opt*. **158**, 1240.

ABEDI-VARAKI, M. & JAFARI, S. 2018*b* Enhanced THz radiation from beating of two Cosh–Gaussian laser beams in a wiggler-assisted collisional magnetized plasma. *J. Opt. Soc. Am.* B **35** (5), 1165.

ABEDI-VARAKI, M. & JAFARI, S. 2018*c* Second-harmonic generation of a linearly polarized laser pulse propagating through magnetized plasma in the presence of a planar magnetostatic wiggler. *Eur. Phys. J. Plus* **133** (4), 137.

ABEDI-VARAKI, M. & KANT, N. 2022 Magnetic field-assisted wakefield generation and electron acceleration by Gaussian and super-Gaussian laser pulses in plasma. *Mod. Phys. Lett.* B **36** (07), 2150604.

ABEDI-VARAKI, M. & PANAHI, N. 2019 Non-linear absorption of an intense laser pulse propagating in wiggler-assisted underdense collisional plasma. *Contrib. Plasma Phys*. **59** (9), e201900001.

ALBERT, F., LEMOS, N., SHAW, J., POLLOCK, B., GOYON, C., SCHUMAKER, W., SAUNDERS, A., MARSH, K., PAK, A. & RALPH, J. 2017 Observation of betatron x-ray radiation in a self-modulated laser wakefield accelerator driven with picosecond laser pulses. *Phys. Rev. Lett*. **118** (13), 134801.

CAIZERGUES, C., SMARTSEV, S., MALKA, V. & THAURY, C. 2020 Phase-locked laser-wakefield electron acceleration. *Nature Photonics* **14** (8), 475.

CHEN, P., CHANG, F.-Y., LIN, G.-L., NOBLE, R.J. & SYDORA, R. 2009 A new type of plasma wakefield accelerator driven by magnetowaves. *Plasma Phys. Control. Fusion* **51** (2), 024012.

ESAREY, E., SCHROEDER, C. & LEEMANS, W. 2009 Physics of laser-driven plasma-based electron accelerators. *Rev. Mod. Phys*. **81** (3), 1229.

FALLAH, R. & KHORASHADIZADEH, S. 2019 Electron acceleration by Bessel–Gaussian laser pulse in a plasma in the presence of an external magnetic field. *High Energy Density Phys*. **31**, 5.

GOPAL, K., GUPTA, D., JAIN, A., HUR, M.S. & SUK, H. 2021*a* Investigation of electron beam parameters in laser wakefield acceleration using skewed laser pulse and external magnetic field. *Curr. Appl. Phys*. **25**, 82.

https://doi.org/10.1017/S0022377823000144 Published online by Cambridge University Press

Gopal, K., Gupta, D.N. & Suk, H. 2021*b* Pulse-length effect on laser wakefield acceleration of electrons by skewed laser pulses. *IEEE Trans. Plasma Sci*. **49** (3), 1152.

Górska, K. & Penson, K.A. 2013 Exact and explicit evaluation of Brézin–Hikami kernels. *Nucl. Phys.* B **872** (3), 333.

Gupta, D., Gopal, K., Nam, I., Kulagin, V. & Suk, H. 2014 Laser wakefield acceleration of electrons from a density-modulated plasma. *Laser Part. Beams* **32** (3), 449.

Gupta, D., Kant, N. & Singh, K. 2018 Electron acceleration by a radially polarized laser pulse in the presence of an intense pulsed magnetic field. *Laser Phys*. **29** (1), 015301.

Haines, B.M., Shah, R.C., Smidt, J.M., Albright, B.J., Cardenas, T., Douglas, M.R., Forrest, C., Glebov, V.Y., Gunderson, M.A. & Hamilton, C.E. 2020 Observation of persistent species temperature separation in inertial confinement fusion mixtures. *Nature Commun*. **11** (1), 1–9.

Hooker, S.M. 2013 Developments in laser-driven plasma accelerators. *Nature Photonics* **7** (10), 775.

Hooker, S., Brunetti, E., Esarey, E., Gallacher, J., Geddes, C., Gonsalves, A., Jaroszynski, D., Kamperidis, C., Kneip, S. & Krushelnick, K. 2007 GeV plasma accelerators driven in waveguides. *Plasma Phys. Control. Fusion* **49** (12B), B403.

Hörmander, L. 1967 Hypoelliptic second order differential equations. *Acta Math*. **119** (1), 147.

Jha, P., Saroch, A. & Mishra, R.K. 2013 Wakefield generation and electron acceleration by intense super-Gaussian laser pulses propagating in plasma. *Laser Part. Beams* **31** (4), 583.

Joshi, C. 2007 The development of laser-and beam-driven plasma accelerators as an experimental field. *Phys. Plasmas* **14** (5), 525.

Joshi, C., Corde, S. & Mori, W. 2020 Perspectives on the generation of electron beams from plasma-based accelerators and their near and long term applications. *Phys. Plasmas* **27** (7), 070602.

Kautz, E.J., Phillips, M.C. & Harilal, S.S. 2020 Unraveling spatio-temporal chemistry evolution in laser ablation plumes and its relation to initial plasma conditions. *Analyt. Chem*. **92** (20), 13839.

Leemans, W., Gonsalves, A., Mao, H.-S., Nakamura, K., Benedetti, C., Schroeder, C., Tóth, C., Daniels, J., Mittelberger, D. & Bulanov, S. 2014 Multi-GeV electron beams from capillary-discharge-guided subpetawatt laser pulses in the self-trapping regime. *Phys. Rev. Lett*. **113** (24), 245002.

Li, Y., Lee, H. & Wolf, E. 2004 New generalized Bessel–Gaussian beams. *J. Opt. Soc. Am.* A **21** (4), 640.

Lindberg, R., Charman, A., Wurtele, J. & Friedland, L. 2004 Robust autoresonant excitation in the plasma beat-wave accelerator. *Phys. Rev. Lett*. **93** (5), 055001.

Litos, M., Adli, E., An, W., Clarke, C., Clayton, C., Corde, S., Delahaye, J., England, R., Fisher, A. & Frederico, J. 2014 High-efficiency acceleration of an electron beam in a plasma wakefield accelerator. *Nature* **515** (7525), 92.

Lundh, O., Lim, J., Rechatin, C., Ammoura, L., Ben-Ismaïl, A., Davoine, X., Gallot, G., Goddet, J.-P., Lefebvre, E. & Malka, V. 2011 Few femtosecond, few kiloampere electron bunch produced by a laser–plasma accelerator. *Nat. Phys*. **7** (3), 219.

Malik, H.K., Kumar, S. & Nishida, Y. 2007 Electron acceleration by laser produced wake field: pulse shape effect. *Opt. Commun*. **280** (2), 417.

Roussel, R., Andonian, G., Lynn, W., Sanwalka, K., Robles, R., Hansel, C., Deng, A., Lawler, G., Rosenzweig, J. & Ha, G. 2020 Single shot characterization of high transformer ratio wakefields in nonlinear plasma acceleration. *Phys. Rev. Lett*. **124** (4), 044802.

Sherlock, M. & Bissell, J. 2020 Suppression of the Biermann battery and stabilization of the thermomagnetic instability in laser fusion conditions. *Phys. Rev. Lett*. **124** (5), 055001.

Tajima, T. & Dawson, J. 1979 Laser electron accelerator. *Phys. Rev. Lett*. **43** (4), 267.

Tajima, T. & Malka, V. 2020 Laser plasma accelerators. *Plasma Phys. Control. Fusion* **62** (3), 034004.

Yadav, M., Gupta, D.N. & Sharma, S.C. 2020 Electron plasma wave excitation by a q-Gaussian laser beam and subsequent electron acceleration. *Phys. Plasmas* **27** (9), 093106.

Zhao, Y., An, W., Xu, X., Li, F., Hildebrand, L., Hogan, M.J., Yakimenko, V., Joshi, C. & Mori, W.B. 2020 Emittance preservation through density ramp matching sections in a plasma wakefield accelerator. *Phys. Rev. Accel. Beams* **23** (1), 011302.